THESIS FOR THE DEGREE OF LICENTIATE OF ENGINEERING

High Performance Cooling Traction Brushless Machine Design for Mass Production

ALESSANDRO ACQUAVIVA

Department of Electrical Engineering
Division of Electric Power Engineering
CHALMERS UNIVERSITY OF TECHNOLOGY
Gothenburg, Sweden 2019

High Performance Cooling Traction Brushless Machine Design for Mass Production
ALESSANDRO ACQUAVIVA

Licentiante Thesis at the Chalmers University of Technology

Department of Electrical Engineering
Division of Electric Power Engineering
Chalmers University of Technology
SE–412 96 Göteborg
Sweden
Telephone +46 (0)35704363

Chalmers Bibliotek, Reproservice
Gothenburg, Sweden 2019

High Performance Cooling Traction Brushless Machine Design for Mass Production

ALESSANDRO ACQUAVIVA
Department of Electrical Engineering
Chalmers University of Technology

Abstract

In the last few years electric vehicles (EVs) are coming on the market. The shift from niche market to main stream is challenging. It took many years to reach the current internal combustion engine quality in the manufacturing process. However, a much faster process is needed for the electric drive-train if sustainability goals about CO_2 emissions are to be met.

It is extremely important to think about the manufacturing process during the design of a piece of hardware if this is meant for mass production. In a few years from now, traction electric motors for EVs will be produced with the rate of millions per year and ensuring a simple, effective and reliable manufacturing process is key in the success of the electric vehicle industry.

This thesis presents an innovative brushless machine design meant for mass production. The machine is designed to achieve high power density and high reliability thanks to a novel cooling concept. The machine selected has a tooth coil winding, also defined as non-overlapping fractional slot concentrated winding. This winding concept is state of the art for many applications with high volumes and powers below 10 kW. Also, these have been proven successful in high power applications such as wind power generators. In this thesis the ambition is to show that this technology is promising as well for traction machines and it presents certain unique advantages when it comes to manufacturing and cooling.

The traction machine in this work is designed for a small two-seater electric vehicle but could as well be used in a parallel hybrid.

Index Terms: Cooling, energy efficiency, electrical machine design, permanent magnet synchronous machine (PMSM).

Acknowledgements

I gratefully acknowledge The Swedish Energy Agency for the financial support.

I would like to thank Prof. Torbjörn Thiringer and Prof. Sonja Lundmark for supervising my work, giving me the freedom of choosing my own research path and making this project possible. I would also like to thank Dr. Emma Grunditz and Prof. Oskar Wallmark for their valuable time and contributions.

Finally, I would like to thank my family for always supporting my choices no matter how far from home I get.

Alessandro Acquaviva
Gothenburg, Sweden
February, 2019

Contents

Introduction

1.1 Problem background

The market for electric vehicles (EV) is strong, with an annual market growth rate above 40 % year-on-year from 2010 [1]. Furthermore, in the past few years, some of the main car manufacturers have declared a shift to only producing cars with electrified drivetrains.

In a few years from now, traction electric motors for EVs will be produced with the rate of millions per year and ensuring a simple, effective and reliable manufacturing process is key to succeed in the electric vehicle industry. It took many years to reach the current quality for the manufacturing process of the internal combustion engine. However, a much faster development is needed for the electric drive-train if sustainability goals about CO_2 emissions are to be met on time.

One important aspect when it comes to power-train design is that components are often highly integrated. The electric machine and the power electronics often share the same cooling loop mainly to reduce complexity and cost of the system. An accurate prediction of the losses of both the machine and converter is crucial for the thermal design of the drivetrain.

The development of electric drivetrains is primarily dominated by the permanent magnet synchronous machine (PMSM) [2], characterized by its high efficiency and high power and torque density capabilities [3, 4, 5]. Also, as torque and power density increase, liquid cooling becomes necessary. A lot of research and industry effort is now dedicated to this and a good overview of the latest solutions in industry can be found in [6, 7].

It is important to think about the manufacturing process during the design of a piece of hardware if this is meant for mass production. Tooth coil winding machines, also defined as non-overlapping fractional slot concentrated winding, are particularly interesting when it comes to high reliability and low manufacturing cost [8, 9, 10]. Tooth coil winding present several opportunities also when it comes to cooling. In [11] a double layer tooth coil winding machine with in-slot cooling between the coils is presented. This solution uses the space in the slot not filled with copper to create cooling. In [12] the authors present a method to reduce harmonic losses for the 12 slot 10 poles machine introducing barriers in the stator that can be used for liquid cooling. Both these concepts are used in the design of the machine in this document.

Missing in literature is a study of how to conduct a design optimization of a tooth coil winding machine with high cooling performance and meant for mass production. Also, missing is literature, is a machine with the combination of both in-slot and direct iron oil cooling.

1.2 Purpose of the thesis and contributions

The purpose of the work presented in this thesis is to show both a general approach to multiphysics modelling of brushless PM machines and a specific design of a traction machine with high cooling capabilities meant for mass production. The intent is to build a prototype to proof the concept and validate the design. The machine is characterized using finite element analysis (FEA) and different control strategies are evaluated.

Two related activities are conducted and presented. Thermal measurements are carried out on a brushless machine with a water cooled jacket and compared to numerical methods. Furthermore, a wide band-gap inverter loss prediction model is presented in the publication list.

The main contributions are the following:

- A method to select pole and slot combinations from both a bottom-up (from performance evaluation of pole slot combinations) and top-down (from the specifications) design criteria for double layer tooth coil winding machines is presented.
- An analytical method to size brushless AC PM machines based on split ratio is presented, showing how with constant current density there is a

clear trade-off between torque density and efficiency, with the cost optimum usually laying in-between.

- A novel cooling design for tooth coil winding machine is presented, with both direct copper and iron cooling.
- A simplified CFD and thermal model of electrical machines with cooling jacket is presented. The computationally efficient simulation model is validated through measurements showing good agreement.
- A quantification and derivation of the energy efficiency consequence of reverse conduction and blanking time for a SiC MOSFET inverter.

1.3 Thesis outline

The thesis is structured to reproduce the steps of the traction machine design process, followed by 4 peer-reviewed conference publications and one submitted journal publication. A detailed outline of the general design methods and processes can be found in the articles presented at the end of the thesis.

In Chapter 2, some theory about tooth coil winding machines and cooling principles is presented. Also, a short review of the state of the art of machine cooling and manufacturing techniques is shown.

Chapter 3 covers the case set up. From the vehicle performance requirements to the drivetrain requirements and in turn the electrical machine and converter design specifications.

Chapter 4, presents the electromagnetic and thermal design procedure of the traction machine.

In Chapter 5, the machine selected is modelled using FEA and CFD and the results are presented and analyzed.

Chapter 6 presents a discussion of the results and the future work to come.

1.4 List of publications

This thesis is based on the work contained in the following papers:

- A. Acquaviva and T. Thiringer - *Energy efficiency of a SiC MOSFET propulsion inverter accounting for the MOSFET's reverse conduction and the blanking time.* Published in *European Conference on Power Electronics and Applications (EPE'17 ECCE Europe)*, Sept., 2017.
- S. Skoog and A. Acquaviva - *Pole-Slot Selection Considerations for Double Layer Three-phase Tooth-Coil Wound Electrical Machines.* Published in *International Conference on Electrical Machines (ICEM)*, September 3-6, 2018.
- A. Acquaviva - *Analytical Electromagnetic Sizing of Inner Rotor Brushless PM Machines Based on Split Ratio Optimization.* Published in *International Conference on Electrical Machines (ICEM)*, September 3-6, 2018.
- S. Lundmark, A. Acquaviva and A. Berqvist - *Coupled 3-D Thermal and Electromagnetic Modelling of a Liquid-cooled Transverse Flux Traction Motor.* Published in *International Conference on Electrical Machines (ICEM)*, September 3-6, 2018.
- A. Acquaviva, O. Wallmark, S. Lundmark, E. Grunditz and T. Thiringer - *Computationally Efficient Modeling of Electrical Machines with Cooling Jacket.* Submitted to IEEE Transactions on Industrial Electronics

Electrical Machines Manufacturing and Cooling

2.1 State of the Art of Traction Electrical Machines

Traction electric drives can be categorized by the electrical machines in use, mainly induction machines and brushless synchronous machines. Currently there is no technology that is proven best. The brushless machine typically presents higher efficiency, power factor and power density compared to the induction machine. However, the efficiency of the induction machine can improve significantly with copper rotor bars, shown in Fig. 2.1. The induction machine does not have magnets, which makes it more reliable since it can not get demagnetized and it is cheaper since no rare earth materials are needed. Furthermore, there is no back electromotive force (EMF) unregulated over-voltage in case of a fault.

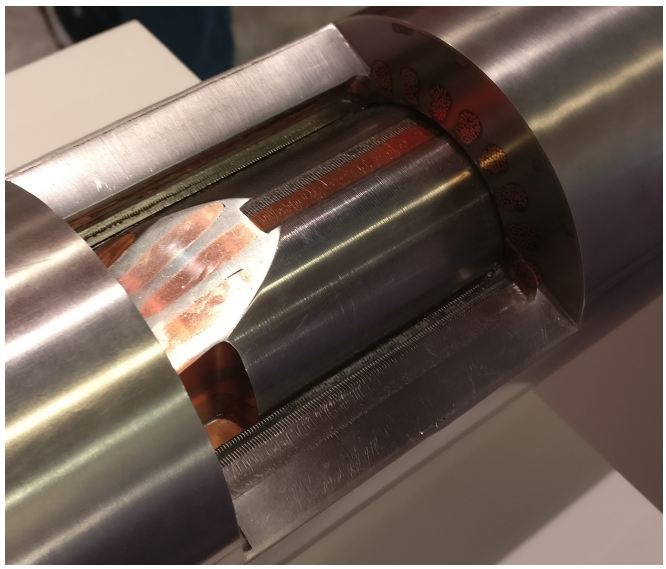

Figure 2.1: Induction machine copper bar rotor

The most found in industry is the brushless ac machine [2]. Brushless ac machines can be further divided either by the rotor type or by their winding type. The former presents many alternatives but mainly interior PM, surface mounted PM and PM assisted synchronous reluctance motor are used. As for the winding types there are two main alternatives, distributed winding and tooth coil winding. These two types of machines are comparable in performance.

One type of distributed winding which is currently state of the art in many traction applications is the hair-pin winding, shown in Fig. 2.2. This presents a simplified manufacturing process by insertion and good fill factors. However, this technology is limited only to a low number of turns, it requires welding at the end connections which complicates the manufacturing and can present problems of ac losses in the conductors for high rotational speeds, i.e. at high frequencies.

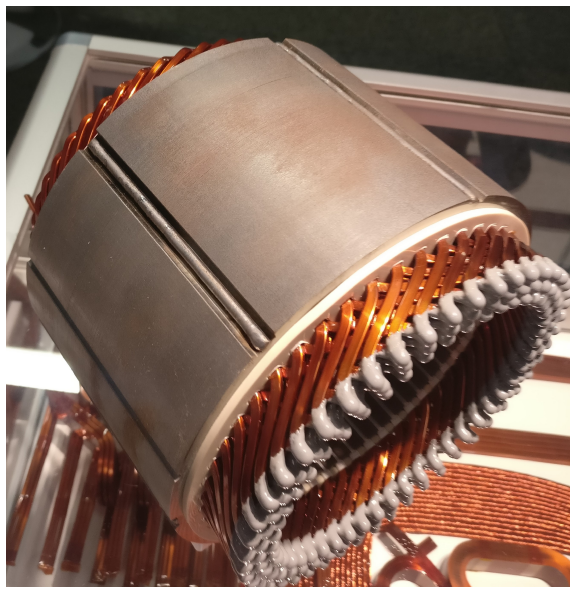

Figure 2.2: Hairpin winding

2.2 Tooth Coil Winding

Tooth-coil wound machines, also known as non-overlapped fractional slot concentrated winding (FSCW) synchronous machines, offer several benefits compared to machines with a distributed winding, but they also present some special characteristics resulting in design challenges not typical for classical distributed winding machines.

The tooth coil winding presents the following advantages:

- Short end windings
- Low noise and torque ripple [8, 9] (this depends very much from pole slot combination)
- Low manufacturing cost [10]
- High slot fill factor achievable especially if used in combined with segmented stator (SMC, Plug-in teeth or Joint-lapped core) [8, 9]
- Better constant power speed range (CPSR) when used with IPM or SPM machines thanks to high values of stator leakage inductance [13, 14]

- Improved fault vulnerability due to lower mutual inductance between phases [13]

While the main issues are:

- Winding factor is lower than 1, which is proportional to the Torque/Ampere ratio [15]
- Space harmonics generate additional losses in rotor iron and PMs, these can be significant, especially at high speeds [8, 9]
- Some pole/slot combinations can produce unbalanced magnetic forces [16]
- Sub-harmonics may cause low dominant vibration modes which may result in high acoustic noise and vibration

When it comes to the production process, tooth coil winding machines present several options. A pole chain stator is shown in Fig. 2.3 and a segmented teeth stator is shown in Fig. 2.4. Some of these options, such as the pole star with yoke ring, single poles with yoke ring and the stator without pole shoes, present the opportunity of pre-winding the coils on bobbins and inserting them. This can reduce greatly the production time and cost by using a spindle winding machine.

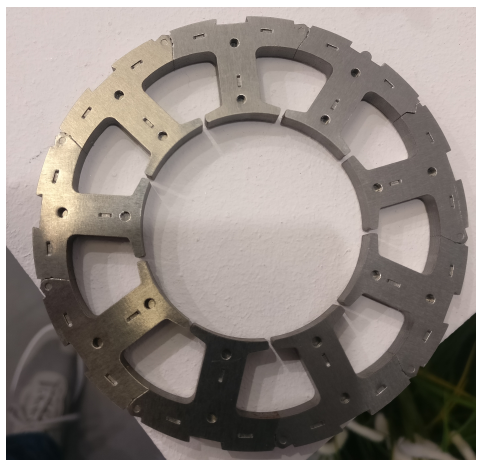

Figure 2.3: Pole chain stator

There are mainly three types of winding machines:

- Spindle winding or linear winding machine
- Flyer winding machine
- Needle winding machine

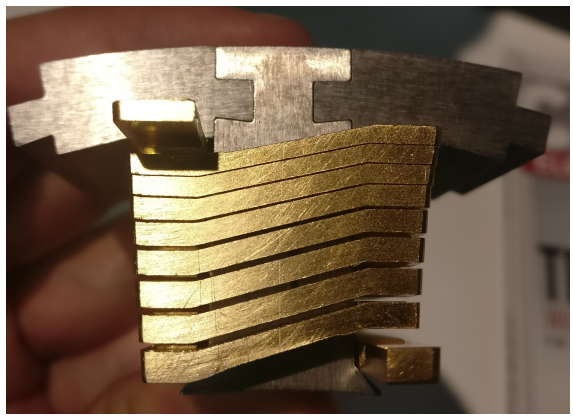

Figure 2.4: Segmented stator

With the spindle winding machine, a coil is produced by winding the wire on a rotating body. This is typically the cheapest and fastest production process, in fact very high rotational speeds can be achieved, especially with thin wires, and many coils can be produced in parallel with a single machine. Using this automatic winding technology on traction machines would greatly reduce the manufacturing cost and time.

2.3 Cooling of Traction Electric Motors and Drive-trains

Traction electric systems are designed for high power density and reliability. In order to achieve this an effective cooling system for the electrical machine is needed, typically a closed loop liquid forced cooling. The main forced cooling solutions found in industry can be categorized as [6, 7]:

- Cooling jacket (water)
- Hallow shaft (oil or water)
- Direct winding cooling (oil)
- Fluid bath (oil)
- Fluid spray (oil)

Some of these are compatible on the same machine.

2.3.1 Oil vs water

Depending on the solution in use there are different options when it comes to the coolant fluid, as shown in [7]. However, most solutions use either oil or water (either pure water or with glycol). The main characteristics of these two coolants are

- Oil has a higher boiling point than water, so it can be used to cool the machine even at a temperature of 100 °C or higher. However, water-cooling may also exceed 100 °C if pressurized.
- Oil is an electrical insulator, thus it can be in direct contact with the winding. Also, a leak from the cooling channel would not cause any hazard. If coolant water should similarly leak, substantial machine damage might occur.
- Oil is already present as a lubricant in the transmission and naturally helps to prevent corrosion.
- The specific heat of water or water/glycol is about twice that of oil, so a given flow rate of water absorbs more heat per degree increase in temperature than the same flow rate of oil.

2.3.2 Direct winding cooling

Direct cooling of the stator winding is an efficient way of cooling, the heat is removed directly at the source. Tooth coil winding, in particular the double layer winding, present particular opportunities of direct winding cooling. The winding is not overlapping which means an easy access to the slot from the end section. Also, in the manufacturing process often some space is left between the two coils, this can be used for the cooling as shown in [11].

Performance Requirements and Design Specifications

In this section the design specifications for the traction machine are derived from the vehicle performance requirements.

3.1 Vehicle description

The reference vehicle is a 2-seater small city car with the performance requirements shown in Table 3.2.

Table 3.1: Vehicle performance requirements

Quantity	Symbol	Value	Unit
Curb weight	m_c	800	kg
Area	A_{vh}	2	m^2
Acceleration 0-100 km/h	-	14	s
Top speed	v_{max}	130	km/h
Aerodynamic Drag Coeff.	C_d	0.3	-
Rolling resistance Coeff.	C_r	0.009	-
Wheel radius	r_w	0.31	m
Starting gradability	-	25	%
Gradability (speed at grade)	-	90 at 6%	$km/h, \%$
Min acceleration	-	1	m/s^2

3.2 Design Specifications

A fixed gear ratio between the axis and the electrical machine is assumed. The gearbox gear ratio is calculated as $G = 10.5$ assuming the base speed of the motor (4500 rpm) at 50 km/h and to reach approximately the maximum allowable speed of 130 km/h. The force and speed requirements and the machine outcome of the sizing process are shown in Fig. 3.1 counting as well for an additional weight of 150 kg (two passengers).

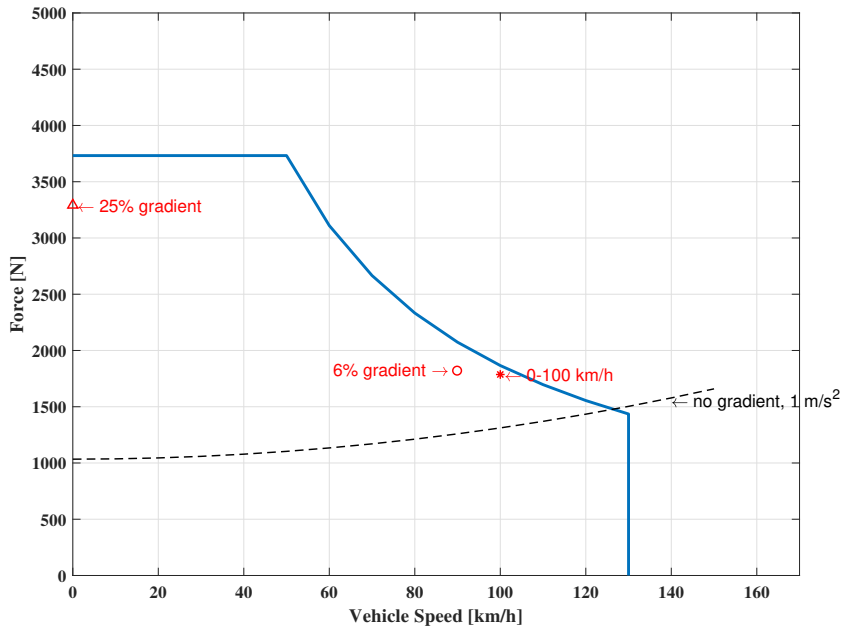

Figure 3.1: Vehicle performance requirements and electrical machine sizing

Standard laminated materials result in reasonable losses with an excitation frequency of 0.1-1.0 kHz. Furthermore, to have a low current ripple the switching frequency is assumed to be at least 20 times the fundamental. If an IGBT converter is used, the converter switching frequency should not exceed 20 kHz to limit the switching losses. The switching frequency can be higher if MOSFETs are used but it is still important to keep the fundamental within a reasonable frequency to limit iron losses. For the reasons above, the maximum fundamental frequency is

set to $f_{f,max} = 1$ kHz. The EM maximum mechanical speed is decided to be

$$n_{max} = \frac{v_{max}}{r_w} G = 12000 rpm. \tag{3.1}$$

The peak torque required by the EM is thus

$$T_{max} = \frac{F_{max,veh}}{r_w G} = 110 Nm. \tag{3.2}$$

The maximum number of pole pairs then becomes

$$p_{max} = \frac{2\pi f_{f,max}}{\omega_{max}} = 5.4. \tag{3.3}$$

where ω_{max} is the EM mechanical maximum angular speed. The EM input design specifications are listed in Table 3.2. As a conservative approach, thanks to the high performance cooling, the machine is sized such that it can withstand the peak conditions indefinitely. The values for maximum temperature of the coolant

Table 3.2: Electrical machine design specifications

Quantity	Symbol	Value	Unit
Peak torque	T_{max}	110	Nm
Peak power	P_{max}	52	kW
Base speed	n_b	4500	rpm
Max speed	n_{max}	12000	rpm
Coolant max Temperature	$\Theta_{max,c}$	60	$^\circ C$
Max winding Temperature	Θ_{max}	180	$^\circ C$
DC bus voltage	V_{dc}	400	V

in Table 3.2 are assumed based on typical values found in industry, the maximum winding temperature is set assuming a class H insulation and the dc bus voltage of 400 V is based on typically used electric vehicles battery voltages.

As a reference, a similar small city car such as the new Smart Fourtwo, which has a curb weight of 880 kg and is available fully electric, mounts a 66 kW synchronous machine.

Design Procedure

4.1 Machine sizing procedure

The sizing procedure used is outlined in [17]. The rotor has been chosen as an internal V shaped PM with air barriers similar to the Toyota Prius electric motor. The reasons for this choice are mainly the saliency which improves the field weakening (FW) characteristic, the robustness of the solution and the lower magnet losses compared to surface mounted thanks to the iron between magnet and the airgap.

A 12 slots 10 poles $p = 5$ machine is chosen based on characteristics listed in [9] as well as the possibility to insert stator barriers as shown in [12] (explained in Section 4.2.1 and shown in Fig. 4.8). Among the characteristics, the most important are: high winding factor (0.933), very low mutual inductance among phases, low cogging and torque ripple.

4.1.1 Design iterations

The solution presented in this report is the outcome of an extensive number of design iterations. The main parameters investigated are:

- Slot and pole number
- Tooth tip presence
- Split ratio, defined as the inner to outer stator diameter ratio $x = D/D_e$
- Magnet coverage of the pole pitch

- Airgap length
- Angle of the V shape
- Airgap flux density

All these parameters have been investigated using the design criteria outlined in [17].

To reach the choice of 12 slot 10 poles, other pole-slot combinations have been evaluated. Three candidates are here compared, a 12 slots 10 poles a 12 slots 8 poles and a 24 slots 8 poles. Figures 4.1 and 4.2 show a comparison of these three machines which have been sized with the procedure as is [17] and using the same input values of torque speed and voltage. Furthermore, the same current density and airgap flux density are set and the machines resulted in similar active volumes. The 12 slot 10 pole machine is the one with higher average torque, lower torque ripple and lower induced voltage distortion. Note that the 12 slots 10 pole machine is without tooth tips while the other two have tooth tips and none of the machines is skewed.

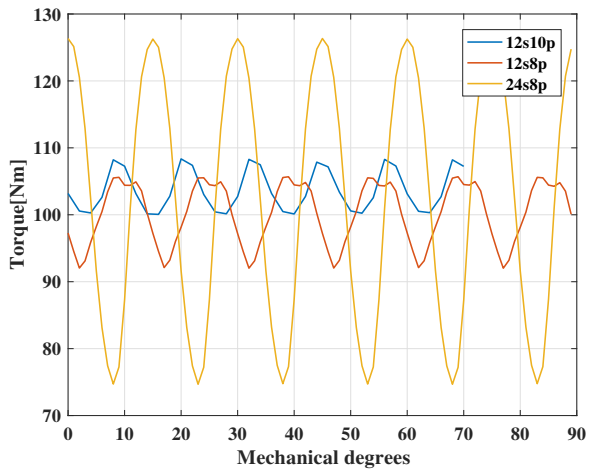

Figure 4.1: Torque of the three machines at maximum torque and base speed of 4500 rpm

A stator design without tooth tip is chosen to improve manufacturing by allowing the coils to be pre-wound and inserted. Several designs with tooth tips have been evaluated. The tooth tip improves the flux linkage, however, if the tooth tip is kept relatively thin to avoid reducing the slot area, at high current the tooth

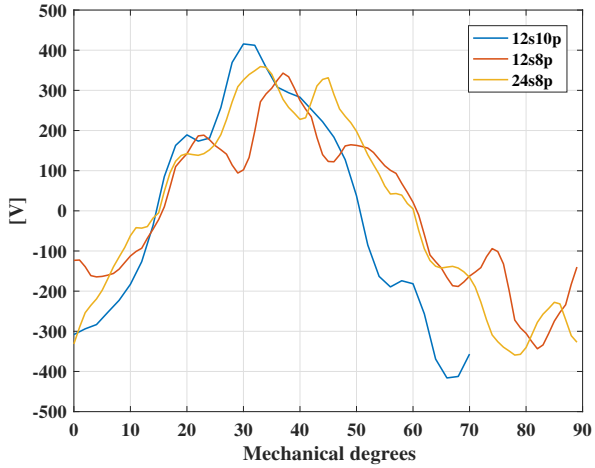

Figure 4.2: Phase to phase voltage of the three machines at maximum torque and base speed of 4500 rpm

tip tends to saturate giving a distorted back EMF. Moreover, the back-EMF shape has a relatively low harmonic content even at high current and in the FW region. The outcome of this investigation resulted in the input data for the analytical sizing listed in Table 4.1. The PMs chosen are NdFeB N48H and the lamination is M250-35A for both stator and rotor.

The outcome of the analytical sizing process is shown in Fig. 4.4, this shows a clear trade-off between torque density and efficiency depending on the choice of the split ratio x. The split ratio chosen is x=0.62. The main reason is to achieve high efficiency. Also, at high current density, if a lower split ratio is chosen, the armature reaction generated by the winding is significant and tends to saturate the machine, as explained in [17]. Furthermore, with a high value of current density chosen as input, slots having a large cross-sectional area are a problem from a thermal perspective. The resulting machine parameters are listed in Table 4.2 and the machine geometry is shown in 4.3.

Table 4.1: Input data and assumptions

Quantity	Symbol	Value	Unit
Airgap	δ	0.7	mm
Ratio length to external diameter	l	0.55	-
Stacking factor	k_s	0.95	-
Copper fill factor	k_{fill}	0.5	-
PM coverage of pole pitch	-	70	%
Angle of the V shape	-	110	°
PM remanence flux densify	B_r	1.2	T
PM relative permeability	μ_r	1.04	-
Max RMS current density	J	33.5	$\frac{A}{mm^2}$
Airgap flux density	B_g	0.9	T
Iron flux density (no load)	B_{Fe}	1.2	T
Max operating temperature	T_{max}	150	$°C$

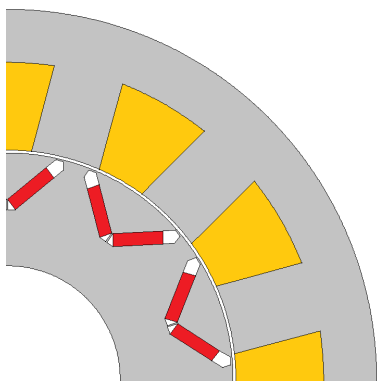

Figure 4.3: Machine outlook before insertion of yoke barriers.

The maximum current is a consequence of, and corresponds to, the maximum current density set in the analytical sizing process. The physical limitation could as well be the current rating of the inverter.

In Fig. 4.5 the disposition of conductors and the shape of the stator are shown, including the cooling channels and the plastic support used to pre-wind the coils.

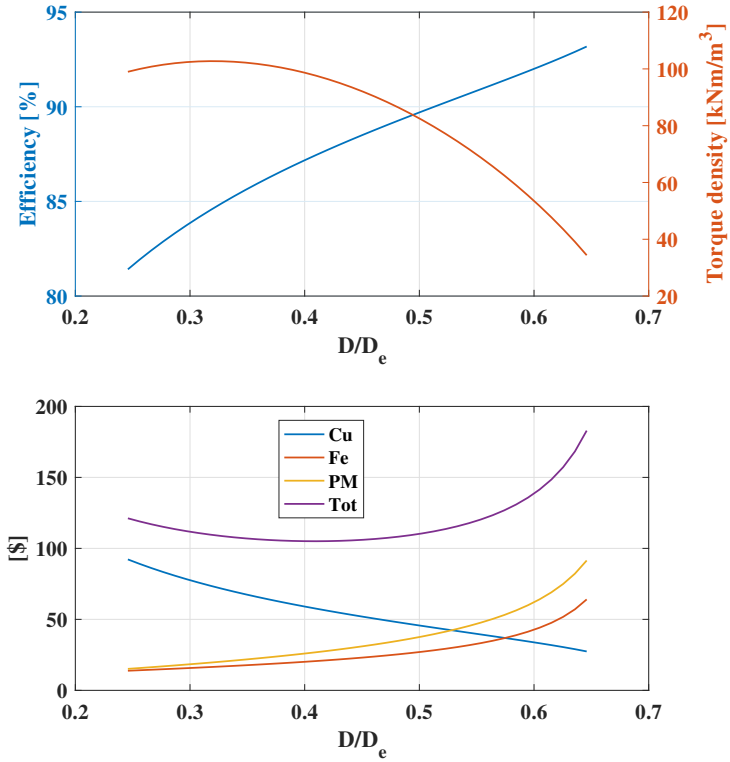

Figure 4.4: Analytical sizing tool output

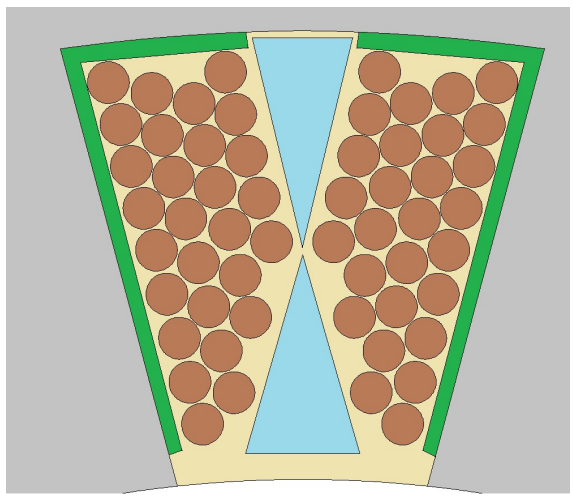

Figure 4.5: Slot design

Table 4.2: Electrical machine main dimensions and data

Quantity	Symbol	Value	Unit
Outer Stator diameter	D_e	180	mm
Inner Stator diameter	D	111.4	mm
Active length	L	100	mm
Tooth width	w_t	17	mm
Stator Yoke width	w_{sy}	13	mm
Magnet thickness	h_m	3.5	mm
Diameter of each conductor	d_N	2	mm
Number of turns per coil	N	28	-
Maximum current	I_{max}	260	A

Note that the coils of each phase are to be connected in parallel with the ones on the opposite side of the stator. The connection diagram for each coil and phase is shown in Fig. 4.6. This choice is made in order to allow a higher number of turns and therefore reduce the size of each conductor which helps improving the manufacturing process (thinner conductors are easier to wind with winding machines).

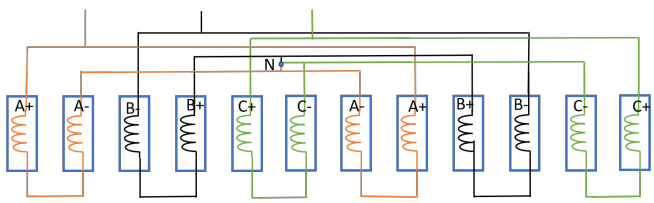

Figure 4.6: Winding disposition and connection

The cooling channels are derived from unused space in the slot. It is important to stress the fact that the coils can be pre-wound on a plastic support and easily inserted thanks to the fact that there is no tooth tip.

The total slot area is 350 mm^2 and the copper area 175 mm^2 so the fill factor is 0.5 as per input value. However, an estimated area of the cooling channels of 80 mm^2 is subtracted from the slot area making the effective fill factor to become 0.65.

The weight of the machine active material is approximately 20 kg and the main material cost around 150 US dollars (considering high volumes).

4.2 Electromagnetic Design

Brushless machines are inverter controlled and have both a voltage and current limit derived from the available dc bus voltage and the current rating of the inverter. The traditional and very intuitive way of defining the machine operating region is to represent it in the d-q current plane. The first step to define the machine operating region is to estimate the machine L_d and L_q inductance. This is done by running two FE simulations at half the rated current, to avoid saturation, and with no PMs (or setting to 0 the remanance flux density in the magnet). The inductance can then be calculated as:

$$L_d = \frac{\Psi_d}{i_d}\bigg|_{i_q=0,\Psi_{pm}=0} \tag{4.1}$$

$$L_q = \frac{\Psi_q}{i_q}\bigg|_{i_d=0,\Psi_{pm}=0} \tag{4.2}$$

From a third FE simulation, with no current, the PM flux linkage can be calculated as

$$\Psi_{pm} = \Psi_d\Big|_{i=0} \tag{4.3}$$

The values obtained at half the rated current are

$$L_d = 0.38mH. \tag{4.4}$$

$$L_q = 0.55mH. \tag{4.5}$$

$$\Phi_{PM} = 0.106Vs. \tag{4.6}$$

Note that the values of inductance reported are already accounting for the effect of paralleling the coils.

From the values of inductance and PM flux linkage the Maximum Torque Per Ampere (MPTA) curve is derived analytically as well as the FW region [18, 19] and are shown in Fig. 4.7 together with the mapping of the machine on the current plane.

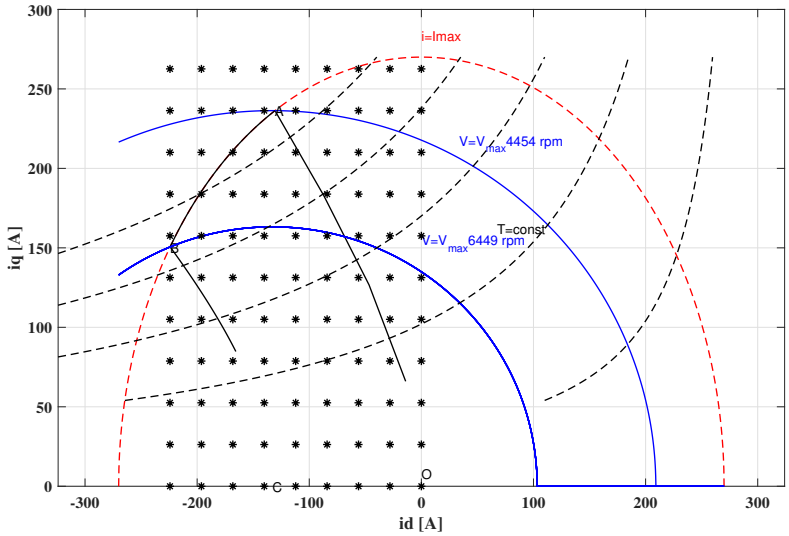

Figure 4.7: Machine mapping and analytical MTPA and FW region

The analytical MTPA and FW regions are used to evaluate the operating region of interest. This area is then mapped using 9 values for the negative d-axis current and 11 values for the q-axis current, resulting in a total of 99 operating points mapped on the current plane. The software used for FEA is FEMM, an open source software [20].

4.2.1 Zero mutual inductance and stator barriers

In [12] a solution to reduce the sub-harmonics in the 12 slots 10 poles machine is presented, this is done using barriers in the stator yoke. A machine with an even key winding factor such as the 12 slot 10 pole machine [9] presents negligible mutual inductance between the phases. This means that the flux generated by a single phase is enclosed between the two adjacent tooth coils and the yoke in-between. A plot of the flux generated by 100 A in phase A and the PMs considered as air is shown in Fig. 4.8. In the yoke in-between coils of different phases there is almost no flux. However, when the PMs flux is added, parts of the PM flux would also flow in-between coils of different phases but still with flux densities below 1.2 T. To sum up, the yoke in between phases is oversized in this design and some barriers for direct iron cooling can be created as shown in Fig. 4.8.

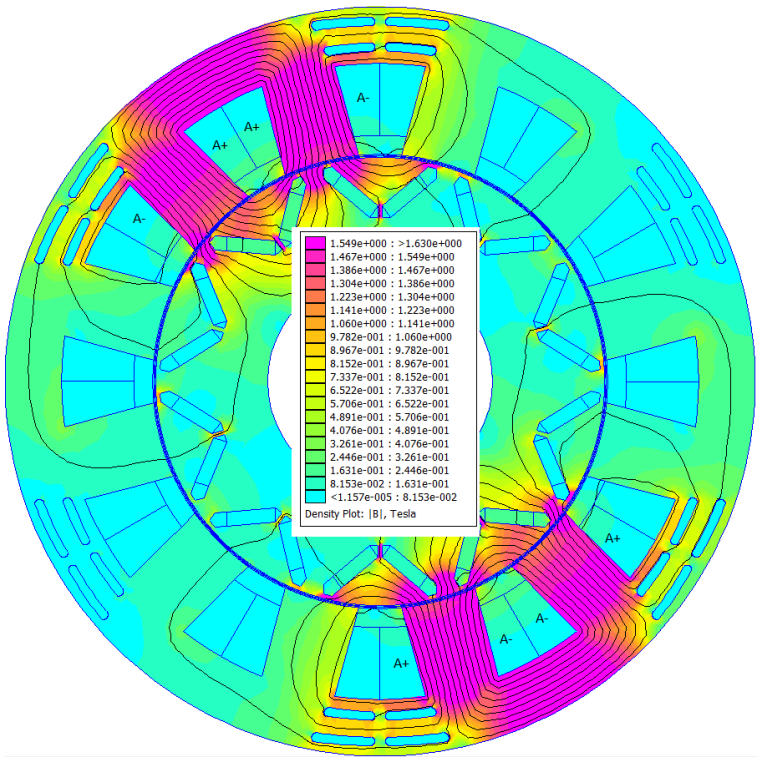

Figure 4.8: Flux generated by 100 A in phase A and no magnets

The same motor geometry with and without barriers has been analyzed at full current and there is no torque reduction due to the barriers.

4.3 Losses

The losses are derived from the 2D FEA analysis with the method presented in [21].

4.4 Thermal Design and Cooling

In this section the thermal behaviour of the motor and the effectiveness of the cooling are analyzed. The losses are calculated from the 2D FEA analysis and

assigned as a heat source in the corresponding 3D domain of the material generating the loss. The procedure is made of three steps:

1. A 3D multiphysics simulation of one slot and one pole of the machine is performed coupling computational fluid dynamic (CFD) and thermal FEM simulations. This is then solved for several flow rates. From the results of these simulations a correlation between the flow rate the and average heat transfer coefficient in the slot cooling channels is derived.
2. A 3D CFD model of both the iron and slot cooling channels as well as the end winding section cooling path is created. The fluid velocity distribution is studied, in particular how the flow rate is distributed among the cooling channels.
3. A thermal 3D model of the complete motor is run with the heat transfer coefficients as boundary conditions using some simplifications as assumptions.

4.4.1 Step 1 - Model to derive heat transfer coefficients

The combined thermal and CFD simulation is built using the the worst case operating point losses as heat sources. The model comprises of only one slot and one pole and all the conductors in the slot are modelled as well as the cooling channels, laminar flow is assumed in the channel. Each component of the losses (PMs, rotor iron, stator iron and copper losses) is distributed over the domain corresponding to the material of the part generating the loss. At the inlet the boundary condition of flow rate is assigned, which corresponds to assigning a constant fluid velocity over the inlet surface. At the outlet a constant pressure is assigned, which is used a reference to evaluate the pressure drop. The input oil temperature in the cooling channel is set to $60°C$. The flow rate is set as the parametric variable sweeping from 1 l/min to 9 l/min. The convection heat transfer coefficient (HTC) can be defined locally for each point on the surface of the cooling channel as

$$h_c = \frac{q}{T_s - T_m} \tag{4.7}$$

where T_s is the temperature of a specific point on the surface, q is the heat flux and

$$T_m = \frac{\int_{A_c} uTdA_c}{u_{avg}A_c}. \tag{4.8}$$

The temperature T_m represents the rate at which thermal energy is advected with the fluid as it moves along the tube [22], A_c is the pipe cross section area available

for flow and u_{avg} is the average velocity of the fluid over the cross section.

One of the shafts sides is set at a constant temperature of 70°C and a small layer of air between the shaft and rotor iron of 0.03 mm is considered. The boundary layer has been assigned using the thin layer approximation built in the software COMSOL in a similar way as in [21]. A boundary condition for the natural convection is assigned to the outer part of the stator on a horizontally displaced cylinder with a length equal to the active length of the machine, which is also a built-in function of COMSOL. The sides of the rotor and PMs have also been assigned a boundary condition of forced external convection with a convection coefficient of 30 W/(m^2·K) to simulate side convection.

The material properties used in the thermal model are reported in Table 4.3.

Table 4.3: Thermal conductivity of materials

Material	λ_{xy}/λ_z or λ [W/(m·K)]
Stator and rotor Lamination	28/2
Aluminum Frame - A356 Temper-T6	128
Magnets - NdFeB	9
Steel shaft - AISI 4340	44.5
Copper drawn wire	287
Slot filler - Resin/Epoxy	1.5
Bobbin	0.8

4.4.2 Step 2 - CFD to check flow distribution

The focus of this second step is to study the flow in the end section and how the flow rate is divided among the cooling channels. The model includes two slots and one end section connecting the two as well as one stator yoke cooling barriers.

4.4.3 Step 3 - Thermal FEA to verify operating conditions

In this last step, the temperature distribution on each part of the motor is analyzed to check that it does not exceed the allowed temperature. The HTCs derived in step 1 are assigned as a boundary condition in the different cooling channels as a function of the flow rate and depending on how the flow splits among the channels (which is checked in step 2).

The conductors and slot filler are modelled with a unified material as in [23]. A model is derived that predicts the equivalent thermal conductivity of a composite material consisting of aligned, infinitely long, equi-sized, rigid, circular cylinders (i.e., the copper conductors) randomly distributed in a medium with lower conductivity (i.e., slot filler and conductor isolation). This value of thermal conductivity is used for the plane parallel to the lamination (referred as x and y directions), while the conductivity of copper is used in the axial directions (referred as z direction). This method allows to avoid modelling each conductor and to decrease the complexity of the model.

The air in the rotor has been modelled with an equivalent thermal conductivity to account for the convection effect at a given speed based on [24] and the air properties at a pressure of 1 atm are taken from [25].

Analysis of Selected Machine

In this chapter the proposed traction machine performance is analyzed using numerical methods as outlined in Chapter 4.

5.1 Flux density and inductance

A plot of the flux density amplitude at the maximum current is shown in Fig. 5.1. The peak flux density in the stator iron is approximately 1.6 T with the exception of the teeth corners which can reach higher values. The stator iron is well utilized considering that above 1.7 T the saturation for the chosen lamination material becomes relevant.

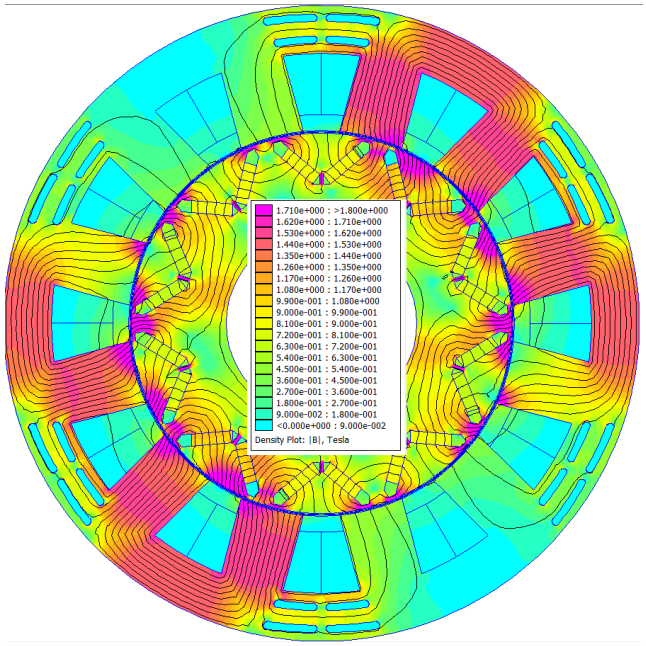

Figure 5.1: Flux density amplitude at maximum current

The d and q axis inductance as function of current are shown in Fig. 5.2.

5.2 Torque and power

The torque achieved in the different operating points is shown in Fig. 5.3. From the figure it is possible to observe that the machine is saturating for high values of q current.

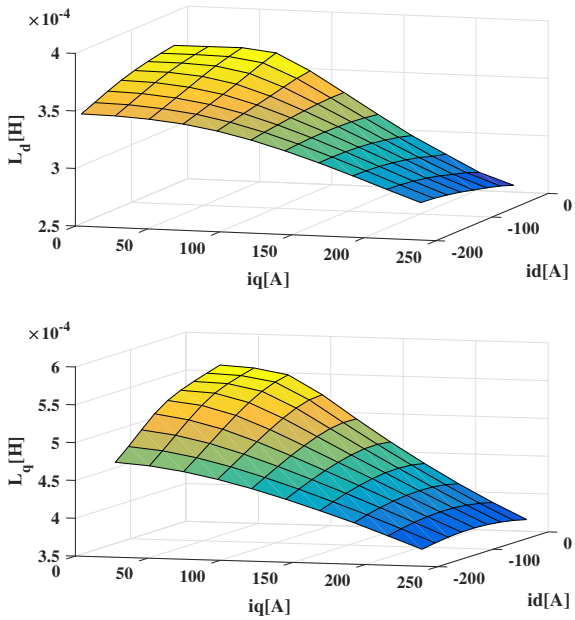

Figure 5.2: d-axis and q-axis inductance as a function of current.

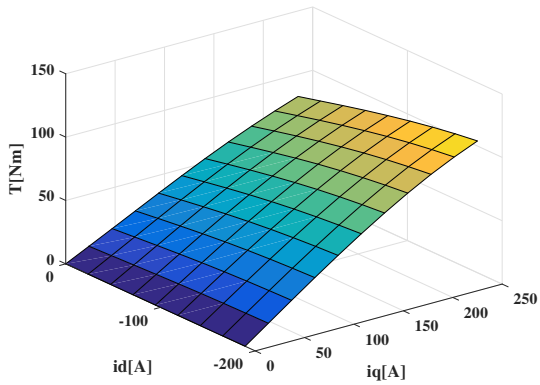

Figure 5.3: Torque as a function of current

In order to evaluate the machine performance four operating points are selected:

1. No load at base speed
2. Half maximum torque at base speed
3. Maximum torque at base speed
4. Maximum speed and available maximum torque in FW

The operating points are shown in Fig. 5.4.

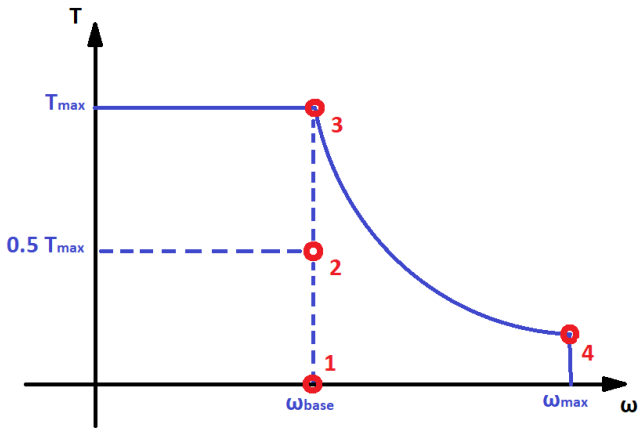

Figure 5.4: Operating points used for evaluation of machine torque and induced voltage

The motor presents very low cogging torque (0.01 Nm peak-to-peak) and the torque ripple at half maximum torque is 3.6% and at maximum torque 6.5%. The torque ripple in different operating conditions is shown in Fig. 5.5.

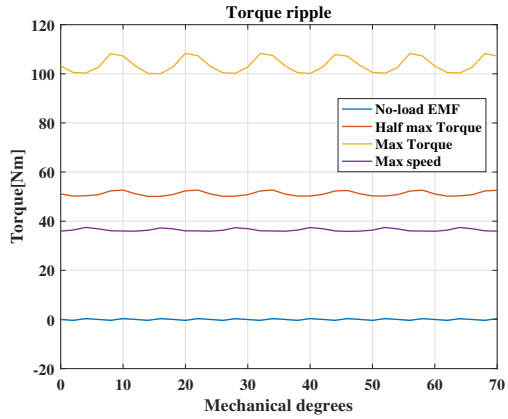

Figure 5.5: Torque ripple in different operating conditions

The power-speed characteristic is shown in Fig. 5.6. The power density of the motor is approximately 2.5 kW/kg (or 19 kW/l) and the torque density is 5.25 Nm/kg.

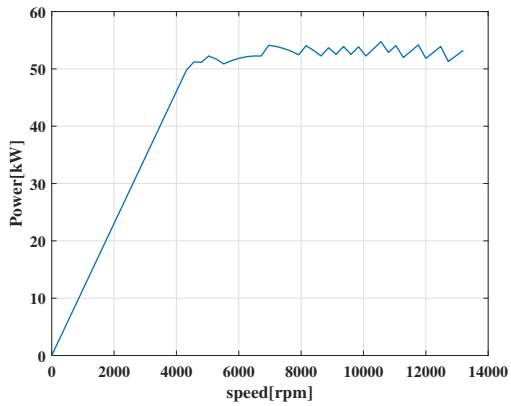

Figure 5.6: Power speed diagram

5.3 Voltage

The no-load back EMF is sinusoidal with a low harmonic content. Both the fundamental and harmonic content of the voltage increase with current due to

inductance and saturation effects caused by the armature reaction. The voltage waveform in different operating conditions together with a Discrete Fourier Transform (DFT) showing the harmonic amplitude with respect to the no-load fundamental is shown in Fig. 5.7.

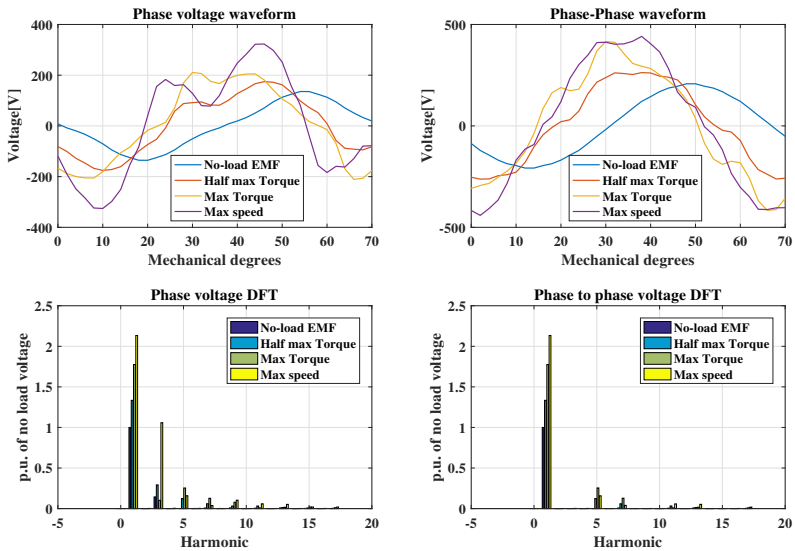

Figure 5.7: Voltage waveform and DFT in different operating conditions

The phase voltage contains a third harmonic which is a problem for a delta connected motor, however the phases in the chosen solution are star connected as shown in Fig. 4.6.

5.4 Losses and Efficiency

The losses are shown in Fig. 5.8. Note that the current is assumed purely sinusoidal which means that the losses due to harmonics present in the current are not considered in this report.

The iron loss distribution is shown in Fig. 5.9 at $i_d = -70A, i_q = 105A$ and $n = 5760$ rpm. The rotor iron losses are very low compared to the stator ones, and the highest loss density can be found on the tooth edges.

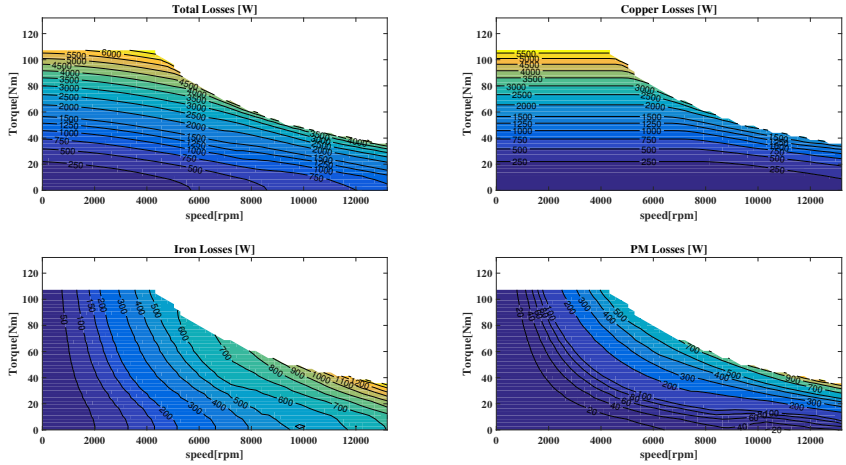

Figure 5.8: Total, copper, iron and PM losses as function of torque and speed

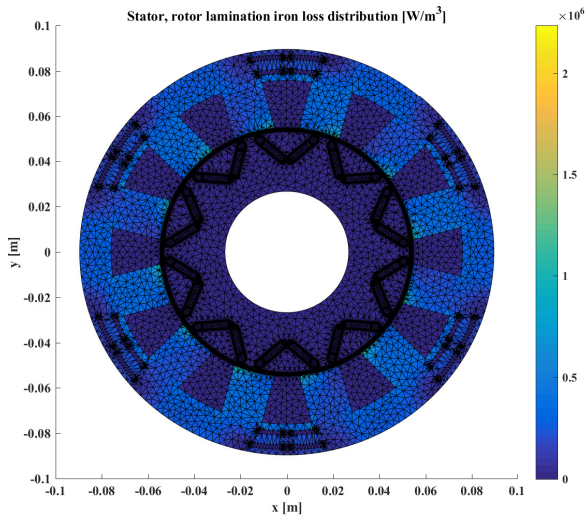

Figure 5.9: Iron loss distribution

The PM loss distribution is shown in Fig. 5.10 for the same operating point and is significantly higher than the stator iron loss distribution in absolute terms.

The PM loss computation assumes that the active length of the magnet is not limiting the current flow or, in other words, the length is greater than the

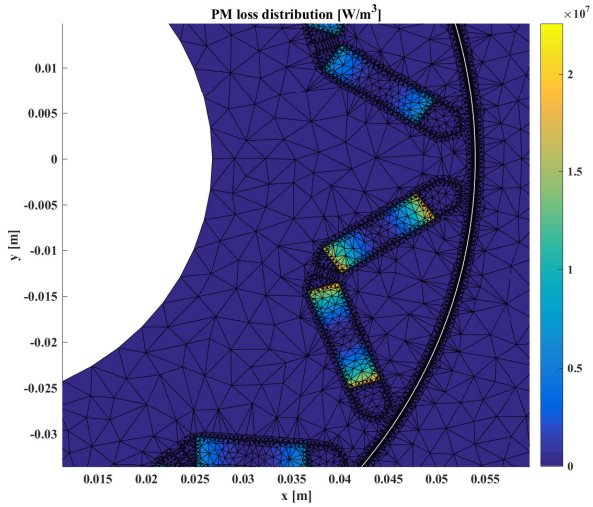

Figure 5.10: PM loss distribution

thickness and width, which is the case for this machine. However, by applying segmentation in the axial direction it is possible to greatly reduce the PM losses. The losses and efficiency plots shown in this report are with solid magnets and the effect of this axial segmentation is not reported. This is because it would be necessary to perform a 3D FEA to account for this effect. The prototype shall have segmented magnets and each segment shall be 10 mm in the axial direction (total of 10 segments) which would greatly reduce the losses in particular in the high torque high speed region. Pre-segmented magnets glued together are available on the market and are the preferred solution for this design.

The electromagnetic efficiency, that does not account for mechanical losses, for both motor and generator operating regions is shown in Fig. 5.11. The peak efficiency is about 95% and, with the exception of the low speed high torque region, the efficiency is above 90%.

5.5 Demagnetization

The machine should be able to withstand a converter fault without being damaged permanently. A severe condition in which the magnets could be permanently demagnetized is when the maximum current is set on the negative d-axis. In order

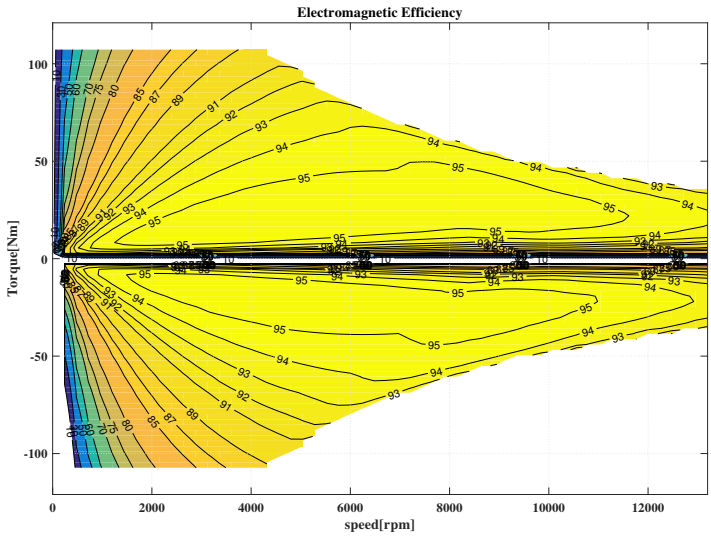

Figure 5.11: Electromagnetic efficiency

to verify that, at the maximum current, the PMs are not demagnetized, a flux density plot set with the maximum amplitude to 0.55 T is shown in Fig. 5.12.

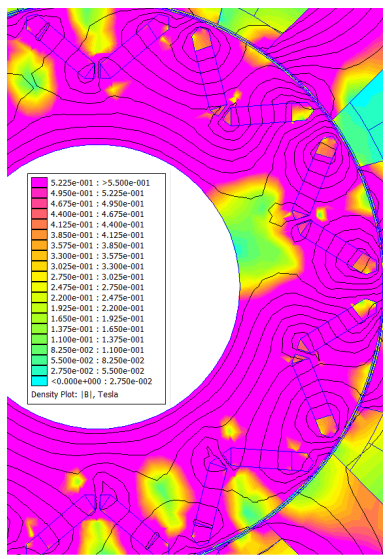

Figure 5.12: PMs flux density with maximum negative d-axis current. The plot maximum flux density is set to 0.55 T to show where it falls below that.

The magnets are of the magenta color indicating that the PM flux density does not fall below 0.55 T. According to the N48H Neodymium-Iron-Boron Magnets BH and HJ curves from the manufacturer's cut sheet, shown in Fig. 5.13, the magnets would not get demagnetized for this fault condition up to a temperature of 120°C.

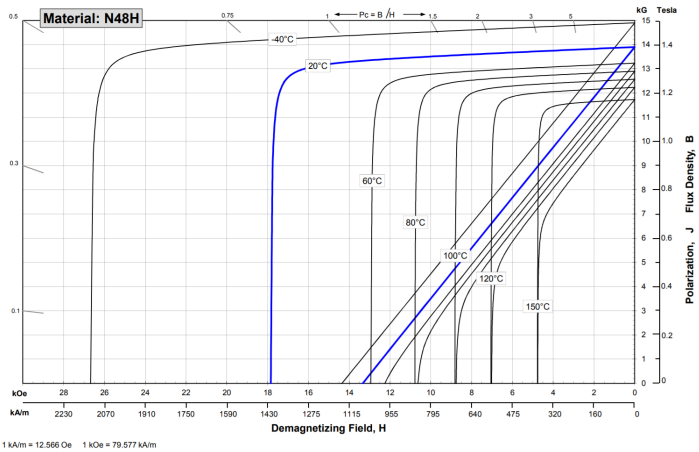

Figure 5.13: Sintered Neodymium-Iron-Boron Magnets - Source: Arnold Magnetics

The three phase short circuit fault at different operating points should also be investigated when studying the demagnetization. However, this is a transient condition and this verification is not performed at this stage.

5.6 Heat transfer coefficient

The heat transfer coefficient on the surface of the cooling channel can be evaluated as explained in the previous chapter. The coolant temperature rise within the single cooling channel in one slot is small. The temperature of the fluid is thus considered constant when it comes to evaluating the convection heat transfer coefficient. The results from step 1 are presented in Fig. 5.14 and the fluid velocity distribution within the slot channels is shown in Fig. 5.15. The fluid is assumed laminar in the cooling channel and this has been confirmed by checking the average Reynolds number.

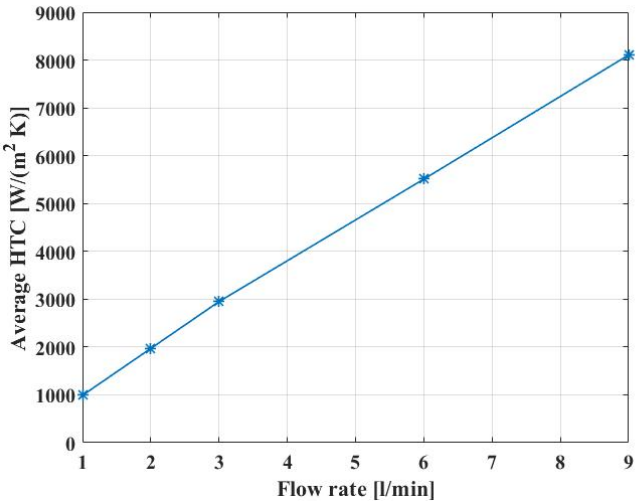

Figure 5.14: Average cooling channel walls convection heat transfer coefficient at different flow rates

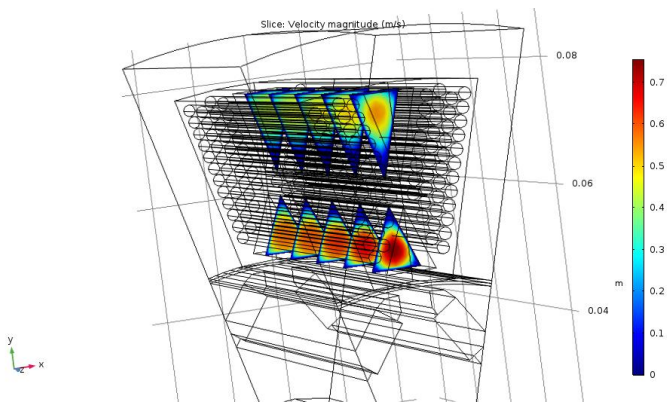

Figure 5.15: Fluid velocity distribution within the slot cooling channel

5.6.1 Flow distribution

As outlined in Chapter 4 the second step is to verify with a pure CFD how the flow rate gets redistributed in the cooling channels. The flow streamlines are shown in Fig. 5.16.

By integrating the velocity over the different channels cross-sections the flow

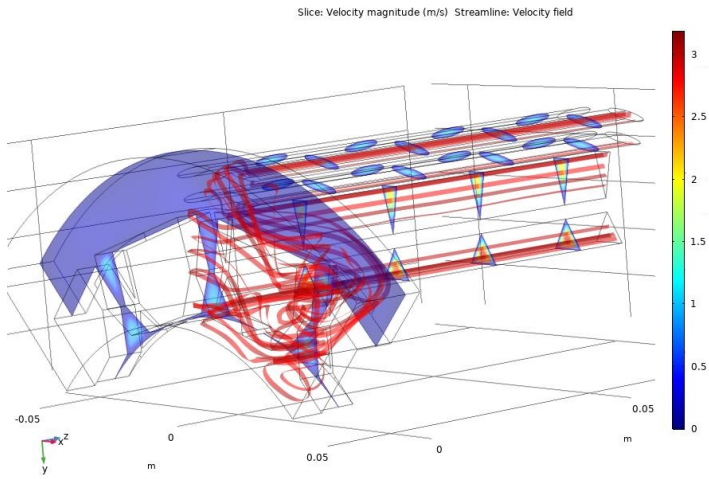

Figure 5.16: Fluid velocity stramlines and flow redistribution among cooling channels.

redistribution can be derived. The flow rate splits evenly between the two in-slot channels. The fluid flow in the end section is turbulent as it can be observed is Fig. 5.16.

5.7 Temperature distribution

In the final step of the thermal analysis of the machine the HTC are assigned as a function of the flow rate as boundary conditions on the walls of the cooling channels. The temperature distribution in a cross section in the middle of the active part of the machine is shown in Fig. 5.17 with a total oil flow rate of 6 l/min.

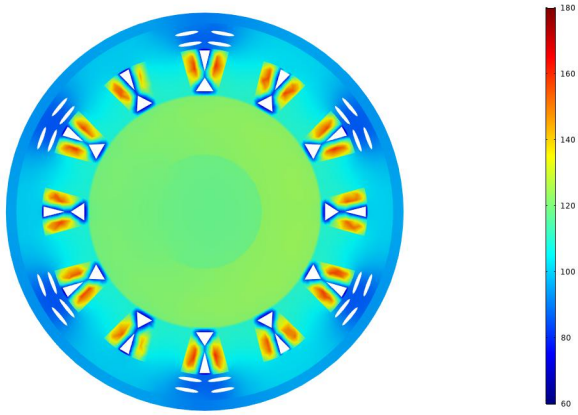

Figure 5.17: Temperature distribution cross section

Figure 5.17 shows that the temperature is within the acceptable range even for the lowest value of flow rate. Considering that the worst case condition is not a continuous condition, the performance of the cooling is well above expectations. The cooling solution presents two parallel paths and the end section would be created by molding the same material of the slot filling. A representation of the end section with the surface temperature distribution is presented in Fig. 5.18.

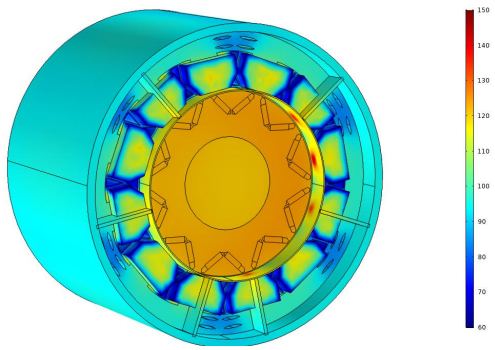

Figure 5.18: End section and surface temperature distribution

The presence of the plastic support in the slot, used to wind the coils, turns out to be beneficial. In fact, it has the effect of limiting the heat flux from copper to iron directing it instead towards the coolant. This is particularly effective for this machine because the copper losses are significantly higher than the rest of the

losses. Furthermore, the cooling channels in the stator yoke allows to remove the heat generated by the iron losses and generated by the rotor.

The thickness of the slot filler material are to be evaluated with more precision during the manufacturing process. These have a significant influence on the thermal behaviour.

To summarize, according to the thermal simulations the machine cooling with a total flow rate of at least 6 l/min can withstand the worst case operating condition indefinitely.

Conclusions

A general approach to multiphysics modelling of brushless PM machines and a specific design of a traction machine with high cooling capabilities meant for mass production is presented in this work. The solution adopted is novel and the intent is to build a prototype to proof the concept and validate the design. The in-slot cooling together with stator yoke cooling barriers show a good thermal behaviour allowing to have high current density and consequently torque density. The machine is designed thinking about the production process of the winding.

6.1 Future Work

The most important future activity is the validation with measurements of the prototype performance and thermal behaviour. The following activities are in progress and will be further analyzed:

- Comparison between water jacket and in-slot oil cooling for traction electric motors.
- Loss model for SiC MOSFET accounting for reverse conduction and blanking time validation with calorimetric measurements.
- Non-isothermal pipe flow modeling in power electronics heatsinks.
- Analysis of effect of eccentricity in brushless machines with different rotor structures.
- Effect of PM losses on torque speed capability of traction brushless AC machines.

- Effect of inverter losses on MTPA and minimum loss control method
- Cooling circuit modelling and analysis on a system level

References

[1] International Energy Agency. Global EV Outlook 2017 [Online]. Accessed 2017-05-14. Available at `https://www.iea.org/publications/freepublications/publication/GlobalEVOutlook2017.pdf`.

[2] E. A. Grunditz and T. Thiringer. Performance analysis of current bevs based on a comprehensive review of specifications. *IEEE Transactions on Transportation Electrification*, 2(3):270–289, Sept 2016.

[3] Juha Pyrhonen, Tapani Jokinen, and Valeria Hrabovcova. *Design of rotating electrical machines*. John Wiley & Sons, 2009.

[4] James R Hendershot and Timothy John Eastham Miller. *Design of brushless permanent-magnet machines*. Motor Design Books, 2010.

[5] K. T. Chau, C. C. Chan, and Chunhua Liu. Overview of permanent-magnet brushless drives for electric and hybrid electric vehicles. *IEEE Trans. on Industrial Electronics*, 55(6):2246–2257, 2008.

[6] Carriero Alberto, Locatelli Matteo, Ramakrishnan Kesavan, Mastinu Gianpiero, and Gobbi Massimiliano. A review of the state of the art of electric traction motors cooling techniques. *SAE Technical Paper*.

[7] Mircea Popescu, David Alan Staton, Boglietti Aldo, Cavagnino Andrea, Hawkins Douglas, and Goss James. Modern heat extraction systems for power traction machines. *IEEE Transactions on Industry Appl.*

[8] Ayman M El-Refaie. Fractional-slot concentrated-windings synchronous permanent magnet machines: Opportunities and challenges. *IEEE Trans. on industrial Electronics*, 57(1):107–121, 2010.

[9] S. Skoog and A. Acquaviva. Pole-slot selection considerations for double layer three-phase tooth-coil wound electrical machines. In *ICEM '18, Alexandroupoli*, 2018.

[10] Florence Libert and Juliette Soulard. Investigation on pole-slot combinations for permanent-magnet machines with concentrated windings. In *Int. Conference on Electrical Machines (ICEM)*, pages 5–8, 2004.

[11] Marcus Schiefer and Martin Doppelbauer. Indirect slot cooling for high-power-density machines with concentrated winding. In *IEMDC '15*, 2015.

[12] Gurakuq Dajaku, Wei Xie, and Dieter Gerling. Reduction of low space harmonics for the fractional slot concentrated windings using a novel stator design. *IEEE Transactions on Magnetics*, 2014.

[13] A. M. El-Refaie, Z. Zhu, T. M. Jahns, and D. Howe. Winding inductances of fractional slot surface-mounted permanent magnet brushless machines. In *Conf. Rec. IEEE IAS Annu. Meeting., Canada*.

[14] F. Magnussen. On design and analysis of permanent magnet synchronous machines for field weakening operation. In *Doctoral Dissertation*, 2004.

[15] F. Magnussen and C. Sadarangani. Winding factors and joule losses of permanent magnet machines with concentrated windings. *IEMDC'03*, 1, 2003.

[16] Z. Q. Zhu, L. M. Jamil, and L. J. Wu. Influence of slot and pole number combinations on unbalanced magnetic force in permanent magnet machines. In *IEEE Energy Conversion Congress and Exposition*, 2011.

[17] Alessandro Acquaviva. Analytical electromagnetic sizing of inner rotor brushless pm machines based on split ratio optimization. In *ICEM '18, Alexandroupoli*, 2018.

[18] W. L. Soong and T. J. E. Miller. Field-weakening performance of brushless synchronous ac motor drives. *IEE Proc.-Electr. Power Appl.*, 141(6):331–340, 1994.

[19] Ching-Tsai Pan and Shinn-Ming Sue. A linear maximum torque per ampere control for ipmsm drives over full-speed range. *IEEE Trans. on energy conversion*, 20(2):359–366, 2005.

[20] D. Meeker. In *2D FEA Open source software, FEMM*.

[21] Emma Grunditz Sonja Lundmark Alessandro Acquaviva, Oskar Wallmark and T. Thiringer. Computationally efficient modeling of electrical machines with cooling jacket. *Submitted to...*, 2019.

[22] Frank Incropera, David Dewitt, Theodore L. Bergman, and Adrienne S. Lavine. *Fundamentals of Heat and Mass Transfer*. John Wiley and Sons, 2007.

[23] G. W. Milton. Bounds on the transport and optical properties of a two-component composite material. *J. Appl. Phys.*, 1981.

[24] J. Nerg, M. Rilla, and J. Pyrhönen. Thermal analysis of radial-flux electrical machines with a high power density. *IEEE Transactions on Industrial Electronics*, 2008.

[25] Y. A. Cengel. *Introduction to Thermodynamics and Heat Transfer*. Mcgraw-Hill, 2008.